

Focusing of light by random scattering

J.M. Vellekoop and A.P.M. Mosk

Complex Photonic Systems, Faculty of Science and Technology,
and MESA⁺ Research Institute, University of Twente,
P.O. Box 217, 7500 AE Enschede, The Netherlands
(Dated: June 21, 2006)

Random scattering of light is what makes materials such as white paint, clouds and biological tissue opaque. We show that although light propagating in these media is diffuse, a high degree of control is possible as phase information is not irreversibly lost. Opaque objects such as eggshell or white paint focus coherent light as sharply as a lens when illuminated with a wavefront that inverts the wave diffusion. We demonstrate the construction of such wavefronts using feedback, achieving a focus that is 1000 times brighter than the diffusely transmitted light. Our results are explained quantitatively by a universal relation based on statistical optics.

PACS numbers: 87.64.Cc, 42.30.Ms, 42.25.Dd

Optical microscopy and spectroscopy are essential tools for the study of living organisms and inanimate objects. These methods rely on the ability to deliver and collect light with a high degree of control. Unfortunately, in many organic and inorganic materials light is scattered randomly and the required directionality of the light is lost [1, 2, 3]. In these materials, light performs a random walk and emerges as a random interference pattern known as speckle. Innovative imaging methods are directed towards isolating the unscattered fraction of the light [4, 5] and towards obtaining useful information from the multiply scattered light [6, 7, 8]. Ideally, one would completely eliminate or counteract scattering.

We demonstrate inverse wave diffusion, a method for counteracting scattering and diffusion of light. By constructing a perfectly matched wavefront, we make normally opaque objects focus light as sharply as a lens. This wavefront cannot be known a priori and is constructed using feedback from a detector in the target focus. By changing the incoming wavefront, we control the position and shape of the focus; it is even possible to transmit collimated beams or simple images. Inverse wave diffusion is universally applicable to scattering objects regardless of their constitution and scattering strength. We envision that, with such active control, random scattering will become beneficial, rather than detrimental, to imaging [9], communication [10, 11] and non-linear optics [12].

Figure 1 shows the principle of the experiment. Normally, incident light from a 632.8 nm HeNe laser is scattered by the sample and forms a random speckle pattern (Fig. 1(a)). The goal is to match the incident wavefront to the sample, so that the scattered light is focused in a specified target area (Fig. 1(b)). We divide the incident wavefront into an array of spatial segments. Initially, the amplitude from each segment contributes randomly to the light amplitude in the target focus (Fig. 1(c)). With a spatial phase modulator, the wavefront of the incident light is adjusted using the intensity in the focus as feedback. The phase of each segment is adjusted until the target intensity is maximal. After adjustment, the phase modulator inverts the diffusion in the sample and

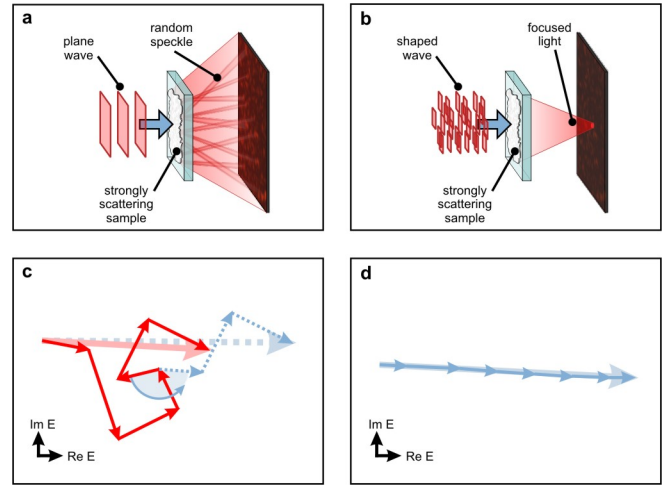


FIG. 1: Design of the experiment. (a) A plane wave is focused on a disordered medium, a speckle pattern is transmitted. (b) The wavefront of the incident light is shaped so that scattering makes the light focus at any desired point. (c) Complex amplitude representation of the field at the target. Before optimization, each segment of the incident wavefront contributes to the field (thick arrow) in a random way. By adjusting the phase of a single segment, we determine the phase at which the total field is maximal (dotted arrows). (d) The phase of the incident light is adjusted to have all fields interfere constructively. The target intensity is at the global maximum.

the scattered light interferes constructively in the target focus (Fig. 1(d)).

We performed first tests of inverse wave diffusion using rutile TiO_2 pigment, which is one of the most strongly scattering materials known. The sample consists of an opaque, 10.1- μm thick layer of white pigment [13] with a transport mean free path of $0.55 \pm 0.10 \mu\text{m}$ measured at a wavelength of 632.8 nm (See Appendix A). Since in this sample the transmitted light is scattered hundreds of times, there is no direct relation between the incident wavefront and the transmitted image [14, 15]. Figure 2 shows the intensity of the transmitted light seen through

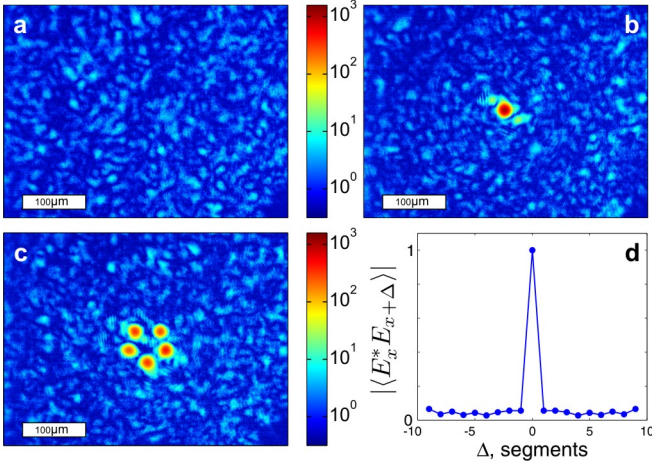


FIG. 2: Shaped transmission through a strongly scattering sample consisting of TiO_2 pigment. (a) Transmission micrograph with an unshaped incident beam. The scattered light forms a random speckle pattern. (b) Transmission after optimization for focusing at a single target. The scattered light is focused to a diffraction limited spot that is 1000 times brighter than the original speckle pattern. (c) Multi-beam optimization. The disordered medium generates very sharp foci at the defined positions. Figures 2(a) to 2(c) are represented on the same logarithmic color scale that is normalized to the average transmission before optimization. (d) Correlation function of the incident wavefront used to form the pentagon seen in Fig. 2(c). There is no correlation between neighboring segments, which indicates that their contributions to the target function are independent. The incident wavefronts are composed of a total of 3228 individually controlled segments.

a microscope objective. In the first image (Fig. 2(a)) we see the pattern that was recorded when a plane wave was focused onto the sample. The transmitted light formed a typical random speckle pattern with a low intensity. We then optimized the wavefront so that the scattered light focused to a target area with the size of a single speckle. The result is seen in Fig. 2(b), where a single bright spot stands out clearly against the diffuse background. The focus was over a factor 1000 more intense than the non-optimized speckle pattern. Instead of focusing light to a single spot, it is also possible to optimize multiple foci simultaneously. By adjusting the target function used as feedback, the scattered light was made to form simple images, such as the pentagon shown in Fig. 2(c). Figure 2(d) shows that there is no correlation between neighboring segments of the optimal incident wavefront, which indicates that the light was fully scattered and no ballistic transmission occurred.

The TiO_2 produced a high quality focus, as can be seen in Figure 3. For comparison, the intensity autocorrelation function of the speckle before optimization is also shown. From statistical optics it is known that the profile of the autocorrelation function equals the diffraction limited beam profile [15]. Since the two functions overlap, we conclude that the multiply scattering TiO_2

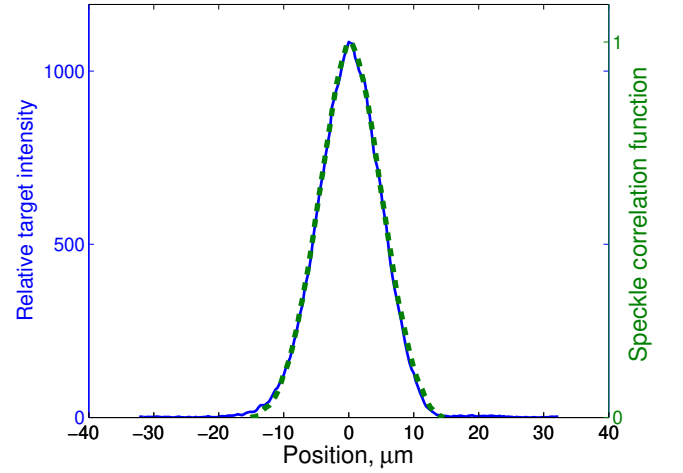


FIG. 3: Cut through the profile of the target focus after optimization (see Fig. 2(b)) compared to the normalized autocorrelation function of the speckle before optimization (dotted line).

Sample	L (μm)	d (μm)	f (mm)	(15%)	N
TiO_2	10.1 0.3	18.7	3.5 0.5	1080	3228
Petal, fresh	43 5	10.6	3.5 0.5	64	208
Petal, dry	37 5	12.6	3.5 0.5	630	1664
Eggshell	430 30	2.1	3.5 0.5	250	3228
Tooth	1500 100	155	125 10	70	208

TABLE I: Intensity enhancement for different materials. L, sample thickness (μm), surface roughness, d, diameter (μm) of focus, f, distance between random medium and focus, μ , maximum enhancement reached, N, number of segments used by the algorithm to describe the wavefront.

produces a diffraction limited focus, i.e. the disordered layer of pigment focuses light as sharply as an ideal lens of the same size. These results are clear proof that the wavefront of multiply scattered transmitted light can be controlled with high accuracy.

Inversion of wave diffusion was realized in a variety of opaque materials ranging from white pigment to fresh flower petals. Table I summarizes the results for the different materials used. Although the samples vary in thickness, composition and scattering strength, they were all able to focus a properly prepared wavefront to a diffraction limited spot. The intensity enhancement – defined as the ratio between the optimized intensity and the average intensity before optimization – varies between 60 and 1000. The main reason for this variation is that the temporal stability of the transmitted speckle pattern is not the same for all materials.

The optimization procedure makes use of the linearity of the scattering process. The transmitted field in the target area, E_m , is a linear combination of the fields

coming from the N different segments of the modulator,

$$E_m = \sum_{n=1}^N t_{m,n} A_n e^{i\phi_n}; \quad (1)$$

where A_n and ϕ_n are, respectively, the amplitude and phase of the light reflected from segment n . All scattering in the sample is described by the elements $t_{m,n}$ of the unknown transmission matrix. Clearly, the magnitude of E_m will be the highest when all terms in Eq. 1 are in phase (also see Fig. 1(c), 1(d)). We determine the optimal phase for a single segment at a time by cycling its phase from 0 to 2π . When the phase of a single segment n is changed, the target intensity detected by the CCD responds as

$$\begin{aligned} |E_m|^2 &= |E_0|^2 + |t_{m,n} A_n|^2 + \\ &2|E_0| |t_{m,n} A_n| \cos[\arg(t_{m,n}) - \arg(E_0) + \phi_n]; \end{aligned} \quad (2)$$

where E_0 is the field of the scattered light originating from all segments except segment n . When N is large, each segment contributes little to the total field and E_0 is equal for all segments. For each segment we store the phase at which the target intensity is the highest. At that point the contribution of segment n is in phase with the already present diffuse background E_0 . After the measurements have been performed for all segments, the phase of the segments is set to their stored values. Now the contributions from all segments interfere constructively and the target intensity is at the global maximum. This method is generally applicable to linear systems and does not rely on time reversal symmetry or absence of absorption.

The maximum intensity enhancement that can be reached is related to the number of segments that are used to describe the incident wavefront. For a disordered medium the constants $t_{m,n}$ are statistically independent and obey a circular Gaussian distribution [15, 16, 17, 18, 19] and the expected enhancement can be calculated,

$$\eta = \frac{1}{4}(N - 1) + 1; \quad (3)$$

It was assumed that all segments of the phase modulator contribute equally to the total incident intensity. We expect the linear scaling behavior to be universal as Eq. 3 contains no parameters. Neither sample thickness nor scattering parameters will influence the expected intensity enhancement. Also, since we are free to choose the basis for Eq. 1, we expect to find the same enhancement regardless of whether the target is a focus or a far-field beam and regardless of how the shaped wavefront is projected onto the sample; of course the required optimal wavefront will be different for these varying configurations. The number of degrees of freedom N is bound to

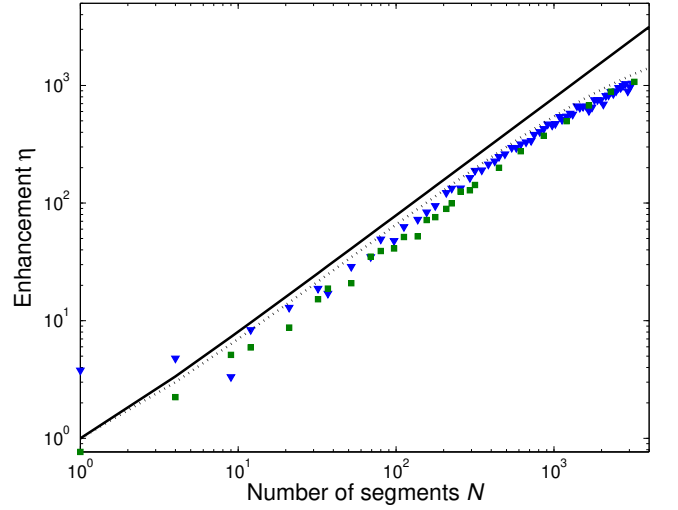


FIG. 4: Enhancement as a function of the number of segments. The experiment was performed twice, once with the sample in focus (squares) and once with the sample 100 μm out of focus (triangles). The solid line represents the theoretical enhancement for an ideal system (Eq. 3). The dotted line represents the expected enhancement when residual amplitude modulation of the phase modulator and the finite persistence time of the sample are taken into account. The uncertainty in η is of the order of the symbol size.

a maximum given by the number independent speckles on the sample surface; $N_{\text{max}} = 8A/\lambda^2$, where A is the illuminated surface area of the sample and λ is the wavelength of the light [18, 19]. When N approaches N_{max} , the intensity in the target focus alone becomes comparable to the total transmission before optimization. In this extremely interesting regime, the assumptions underlying Eq. 3 are no longer valid. With our current apparatus $N \ll N_{\text{max}}$.

We tested the universal scaling behavior implied by Eq. 3 by changing the number of segments into which the phase modulator is subdivided. Using the same TiO_2 sample as before, the algorithm was targeted to construct a collimated beam. In Fig. 4 the enhancement is plotted as a function of the number of segments for different focusing conditions. The linear relation between the enhancement and the number of segments is evident until the enhancement saturates at $\eta \approx 1000$. All measured enhancements were slightly below the theoretical maximum. This is understandable since the phase space is huge and all perturbations move the system away from the global maximum. The main reason for deviations from the optimal wavefront is residual amplitude modulation in the phase modulator. The amplitude modulation introduced a constant, uncontrollable bias in the field (See Appendix A).

The saturation of the enhancement was the result of slow changes in the speckle pattern. This instability effectively limited the number of segments for which the optimal phase could be measured. We estimate that the

effective enhancement decreases to $\epsilon_{\text{eff}} = \epsilon / (1 + N T / T_s)$, where $T = 12$ s is the time needed for one measurement and $T_s = 5400$ s is the timescale at which the speckle pattern of the TiO_2 sample remains stable. The instability of the speckle pattern was most likely caused by a fluctuating humidity of the sample [20]. Depending on the environmental conditions, T_s can be considerably higher and enhancements of over two thousand have been measured overnight.

Our results show that precise control of diode light is possible using an optimal, non-iterative algorithm; light can be directed through opaque objects to form one or multiple foci. The brightness of the focal spot is explained by a model based on statistical optics. We expect inverse wave diffusion to have applications in imaging and light delivery in scattering media. Dynamic measurements in biological tissue are possible when the time required for achieving a focus can be reduced to below 1 ms per segment [4, 6]; we estimate that this timescale is technologically possible with the use of fast phase modulators. Furthermore, the high degree of control over the scattered light should permit experimental verification of random matrix theories for the transport of light and quantum particles [18, 19].

We thank Ad Lagendijk for valuable discussions, Willem Vos and Vinod Subramaniam for a critical reading of the manuscript, and the Photon Scattering group of the Institute for Atomic and Molecular Physics (AMOLF) for providing samples. This work is part of the research program of the "Stichting voor Fundamenteel Onderzoek der Materie (FOM)", which is financially supported by the "Nederlandse Organisatie voor Wetenschappelijk Onderzoek (NWO)".

I. APPENDIX A: MATERIALS AND METHODS

Phase shaping

The experiments are performed using a polarized 5 mW Helium-Neon laser with a wavelength of 632.8 nm. Phase modulation is achieved using a Holoeye LCR-2500 twisted nematic liquid crystal reflective spatial light modulator. The experimental configuration is shown in Figure A1. We illuminate a circular area containing 3×10^5 pixels grouped together in square segments. The phase modulator operates in a phase-only mode [21]. In this mode, the field modulation curve can be closely approximated by a circle in the complex plane. Due to residual amplitude modulation, the centre of this circle is biased with respect to the origin. The bias corresponds to an uncontrollable fraction of 40% of the field. Therefore, the ratio of the controlled intensity to the average total in-

tensity coming from the phase modulator is $1.0^2 / (0.4^2 + 1.0^2) = 0.86$. After each adjustment of the phase, we allow for a stabilization time of 100 ms. The phase shaped beam is spatially filtered to remove higher order diffraction and focused onto the sample using an objective with a magnification of 63 times and a numerical aperture of 0.85. Since the solid angle covered by the objective is 0.95 and only a single polarization is used, at most 24% of the mesoscopic channels can be addressed. A fraction of the phase shaped light is directed to a silicon photodiode which acts as an intensity reference.

Detection

The transmitted light is imaged using a microscope objective with an NA of 0.5 and a magnification of 20 times. The light passes a Glan Thompson polarizer and is detected using a 2/3", 12-bit CCD camera in the back focal plane of the objective. The camera image is integrated over an area that is smaller than the typical speckle size. No collimating optics are used behind the sample. Per segment of the phase modulator, the phase is varied between 0 and 2π in ten equal steps and a sinusoid is fitted to the measured intensities. To minimize the effect of noise, the optimization procedure first performs a coarse pre-optimization using 12 segments. Then, the algorithm is executed twice. The result of the first iteration is used as the reference field for the second iteration. The average intensity of the speckle background is obtained by averaging over 4000 random phase patterns.

Samples

Four different samples were used: TiO_2 , flower petals, egg shell, and a primary tooth. The first sample consists of an opaque, 10.1 μm thick layer of rutile TiO_2 pigment on a 2 mm-thick fused silica substrate [13]. By measuring the total transmission, the transport mean free path was found to be $0.55 \pm 0.10 \mu\text{m}$ at a wavelength of 632.8 nm. The sample was placed with the pigment layer towards the first microscope objective. The flower petal was freshly picked from a *Bellis Perennis* (Common Daisy) and coated with room temperature paraffin between a microscope slide and a coverslip. A second petal was wet mounted on the slide after which the sample was allowed to dry for one day. The egg shell is from a white chicken's egg. A part of the shell was rinsed, dried and placed between the microscope objectives. The primary tooth (incisor) was placed in the focal plane of the first microscope objective. In this latter case, a second objective was not used.

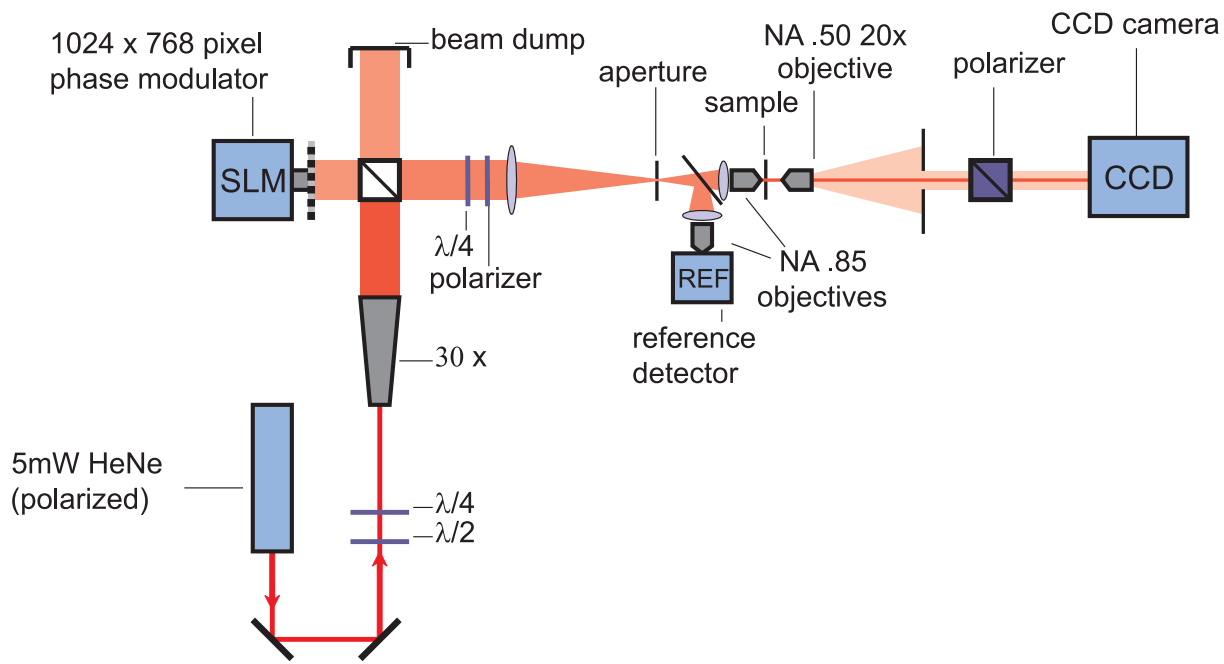


Figure A 1: Schematic drawing of the apparatus.

-
- [1] E. A. Milne, Monthly Not. Roy. Astron. Soc. 81, 361 (1921).
- [2] S. Chandrasekhar, Radiative Transfer (Clarendon Publications, Inc., New York, 1960).
- [3] A. Ishimaru, Appl. Opt. 17, 348 (1978).
- [4] B. J. Vakoc, S. H. Yun, J. F. de Boer, G. J. Teamey, and B. E. Bouma, Optics Express 13, 5483 (2005).
- [5] C. Zhou, G. Yu, D. Furuya, J. H. Greenberg, A. G. Yodh, and T. Durduran, Optics Express 14, 1125 (2006).
- [6] J. Li, G. Detsche, D. Iffime, S. E. Skipetrov, G. Maret, T. Elbert, B. Rockstroh, and T. Giesler, J. Biomed. Opt. 10, 044002 (2005).
- [7] P. Sebbah, ed., Waves and Imaging through Complex Media (Kluwer Academic, Dordrecht, Netherlands, 2001).
- [8] P. N. den Outer, T. Nieuwenhuizen, and A. Lagendijk, J. Opt. Soc. Am. A 10, 1209 (1993).
- [9] O. I. Lobkis and R. L. Weaver, J. Ac. Soc. Am. 110, 3011 (2001).
- [10] A. Derode, A. Tourin, J. de Rosny, M. Tanter, S. Yon, and M. Fink, Phys. Rev. Lett. 90, 014301 (2003).
- [11] S. H. Simon, A. L. Moustakas, M. Stoytchev, and H. Safar, Phys. Today 54, 38 (2001), URL <http://www.aip.org/pt/vol-54/iss-9/p38.html>.
- [12] M. Baudrier-Raybaut, R. Haidar, P. Kupecek, P. Lemasson, and E. Roséncher, Nature 432, 374 (2004).
- [13] R. H. J. Kop, P. de Vries, R. Sprik, and A. Lagendijk, Phys. Rev. Lett. 79, 4369 (1997).
- [14] R. Pappu, B. Recht, J. Taylor, and N. Gershenfeld, Science 297, 2026 (2002).
- [15] J. W. Goodman, Statistical optics (Wiley, New York, 2000).
- [16] N. Garcia and A. Z. Genack, Phys. Rev. Lett. 63, 1678 (1989).
- [17] M. A. Webster, T. D. Gerke, A. M. Weiner, and K. J. Webb, Opt. Lett. 29, 1491 (2004).
- [18] C. W. J. Beenakker, Rev. Mod. Phys. 69, 731 (1997).
- [19] J. B. Pendry, A. MacInnon, and A. B. Pette, Physica A 168, 400 (1990).
- [20] A. Drobniak, K. Rozniakowski, and T. W. Wojtowicz, Quantum Electronics 25, 714 (1995).
- [21] J. A. Davis, J. Nicolas, and A. Marquez, Appl. Opt. 41, 4579 (2002).